

PACS numbers: 52.50.Jm; 52.38. – r
DOI: 10.1070/QE2006v036n07ABEH013173

Formation and development dynamics of femtosecond laser microplasma in gases

V.V. Bukin, N.S. Vorob'ev, S.V. Garnov, V.I. Konov,
V.I. Lozovoi, A.A. Malyutin, M.Ya. Shchelev, I.S. Yatskovskii

***Abstract*. We report our experimental investigations of the formation and development dynamics of laser plasma produced in gas microvolumes (microplasma) upon multiple ionisation by tightly focused (to a spot 2 – 3 μm in diameter) high-intensity (up to $\sim 10^{17}$ W cm^{-2}) femtosecond pulses of a Ti : sapphire laser ($\tau_p \simeq 130$ fs, $\lambda = 800$ nm). Precision interferometric measurements (with a spatial resolution of ~ 1.5 μm) were made of the spatiotemporal distribution of the refractive index and electron density in the microplasmas of the air and helium immediately during the action of the exciting femtosecond laser pulse and at the initial stage of free plasma expansion. The microplasma formation was shown to occur as a result of almost complete (up to bare nuclei) ionisation of the initial gas. For the first time the spectral continuum and the dynamics of spectral line formation in the UV and visible spectral ranges were investigated with a picosecond time resolution for the femtosecond laser-produced microplasmas of the air, N_2, Ar, and He at normal conditions. For the first time the generation of the second (even) laser radiation harmonic was recorded in a femtosecond subcritical-density plasma of gases.**

Keywords: *femtosecond laser plasma, multiple gas ionisation, microinterferometry, spectral-temporal diagnostics, generation of laser harmonics.*

1. Introduction

The study of nonequilibrium laser plasma produced in gases and condensed media ionised by high-intensity ultrashort pulses (USPs) is an important direction in laser radiation – matter interaction physics. This problem is topical from the standpoint of fundamental science – gaining new experimental data on the properties of extremely nonequilibrium, spatially nonuniform high-density plasma and on the mechanisms of its production, development, and interaction with laser radiation. This problem is also topical in connection with numerous applied problems – development of techniques for the generation of extremely short (attosecond) light pulses, development of laser-driven sources of X-ray and UV radiation of the nanometre wavelength range for nanolithography, improvement of the technologies and development of new methods for precision laser micro- and nanostructuring of the surface and volume of metals and transparent optical materials, in which the plasma generated by laser radiation in a gas plays a decisive role.

In this work, we report the main results of experiments carried out to investigate the dynamics of the formation and development of laser plasmas produced at atmospheric pressure in gas microvolumes (the air, nitrogen, argon, helium) by tightly focused (to a region of the order of several micrometres) high-intensity (from $\sim 10^{14}$ W cm^{-2} to $\sim 10^{17}$ W cm^{-2}) femtosecond laser pulses of a Ti : sapphire laser with a duration $\tau_p \simeq 130$ fs, an energy up to 1 mJ, a wavelength $\lambda = 800$ nm, and a nearly Gaussian spatial intensity profile. Such a plasma object with a characteristic diameter of several micrometres and a length up to several tens of micrometres (the so-called microplasma) is an interesting and important object for experimental investigations both in view of the aforementioned basic and applied aspects of this problem and in connection with the unique opportunity to study the behaviour of matter and plasma in superstrong laser fields (of subrelativistic intensity) employing relatively simple and compact femtosecond laser facilities. Indeed, the high quality of Ti : sapphire laser radiation permits focusing the beam to a region ~ 1 μm in diameter and thereby attaining 'in-vacuum' intensities as high as 10^{18} W cm^{-2} even for a pulse energy of about 1 mJ.

Therefore, the microplasma production by high-intensity femtosecond pulses in itself presents no special problems, but its subsequent study encounters serious experimental obstacles and, in the first place, the inadequate readiness of the methods for the investigation of transient microdimensional plasma objects and the ultrafast physical processes occurring therein, including the methods of ultrafast laser microinterferometry and ultrafast microspectroscopy of laser-generated plasmas.

In this work we present the results of our investigations aimed at the development and practical realisation of the methods for microplasma studies. Earlier we reported the technique for precision microinterferometry of micrometre-sized plasmas generated by picosecond laser pulses in gases and optical media (quartz) [1, 2]. More recently this technique was substantially modified and employed to investigate a femtosecond microplasma [3, 4]. In addition we proposed a method for electron-optical recording of the emission spectra of laser-produced microplasma [3 – 6]. The results of its practical application are presented in the

V.V. Bukin, N.S. Vorob'ev, S.V. Garnov, V.I. Konov, V.I. Lozovoi, A.A. Malyutin, M.Ya. Shchelev, I.S. Yatskovskii A.M. Prokhorov General Physics Institute, Russian Academy of Sciences, ul. Vavilova 38, 119991 Moscow, Russia; e-mail: garnov@kapella.gpi.ru

Received 31 March 2006
Kvantovaya Elektronika **36** (7) 638 – 645 (2006)
Translated by E.N.Ragozin

present paper along with microinterferometric measuring data.

2. Precision laser microinterferometry of femtosecond laser plasma

Figure 1 shows the scheme of the technique elaborated and the experimental setup for microinterferometric investigations of the formation and development dynamics of a femtosecond laser microplasma and for measuring its parameters. A single femtosecond pulse of linearly polarised Ti : sapphire laser radiation was split by a beamsplitter mirror into two unequal pulses. The stronger pulse (in what follows, the exciting pulse) was employed for plasma production in the gas under investigation, and the weaker pulse for probing ('strobing') the resultant plasma and for the formation of its interferometric image on the photorecording device. Recall that basically any of the numerous techniques of pulsed laser interferometry employed for plasma diagnostics, which were repeatedly and successfully employed earlier and are currently employed in numerous experimental works (see, for instance, Refs [1, 2, 7–28] and references therein), is based on recording 'instantaneous' interferometric images of the volume of the excited substance (plasma) obtained with the help of probing 'backlighting' laser pulses delayed in time.

The main distinction of our techniques from other techniques consists in its precision – the combination of high temporal ($\sim$100 fs) and spatial ($\sim$1.5 μm) resolution and thereby the capacity to measure the spatiotemporal distribution of the refractive index and electron density of the microplasma, both directly during the exciting laser pulse (at the very initial stage of plasma formation and laser radiation – plasma interaction) and at the stage of its free expansion.

The plasma was produced by focusing the exciting pulse into the volume of the gas under investigation (the air and helium) employing aspherical microlens (*2*) with a focal distance $F = 8$ mm and a numerical aperture NA = 0.5. In this case, the minimal transverse dimension of the focused Gaussian beam was $\sim 2.5 \times 3.5$ μm (at the $1/e^2$ level). We emphasise that the dimensions and spatial intensity profile of the tightly focused beam were carefully measured in our experiments (the measured intensity profiles are given below in Fig. 7). To investigate the dependence of plasma parameters on the energy (intensity) of the exciting pulse, neutral filters were placed in front of the focusing microlens, which ensured attenuation of the pulse energy by a factor of 100 or more, down to the threshold of gas breakdown (which is equal, for instance, for the air to $\sim 2 \times 10^{14}$ W cm^{-2}).

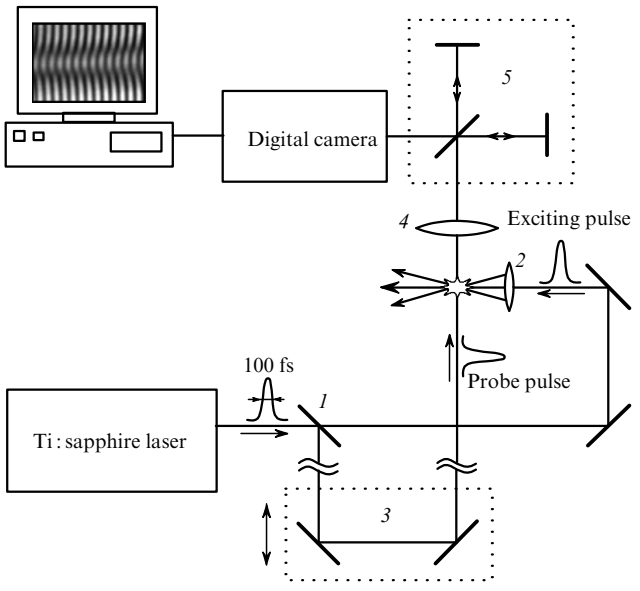

Figure 1. Scheme of the experimental setup for interferometric investigations of the formation and development dynamics of a femtosecond laser microplasma: (*1*) beamsplitter; (*2*) focusing lens ($F = 8$ mm, NA = 0.5); (*3*) adjustable delay line; (*4*) imaging objective lens ($F = 50$ mm, NA = 0.5); (*5*) Michelson interferometer.

The probe pulse was directed to the variable optical delay line; after passing through the delay line, the pulse traversed the microplasma under investigation in the direction perpendicular to the direction of exciting-pulse propagation. The delay time was varied by changing the optical line length with the help of a precision stepping motor from -1 ps to $+10$ ps with a minimal spatial increment of 1.5 μm (which corresponds to a delay time of 10 fs). The variation of the pulse delay over a wider range (over a range of several hundred picoseconds) was effected by manual translation of the optical-line mirror unit along the direction of probe pulse propagation.

A high-quality objective lens ($F = 50$ mm, NA = 0.5) produced the interferometric microplasma image 'in the light' of probing radiation on the light-sensitive CMOS matrix of a digital camera (Elphel Inc., www.elphel.com). To this end, the probing radiation concentrated by the imaging lens was preliminarily directed to a Michelson interferometer to be spit into two coherent beams. Since the radiating microplasma dimensions were much smaller than the probe beam diameter ($\sim$3 mm), its major portion transmitted outside the region of induced optical nonuniformity could be used as the reference beam. In this case, the Michelson interferometer fulfilled the functions of spatial separation of the reference and object beams, selection of the orientation and period of interference fringes, as well as the compensation for the propagation difference between the interfering femtosecond pulses. The requisite accuracy and adjustment stability of interferometer mirrors were effected by way of micrometre linear and angular displacements. The optical magnification M the microplasma image dimension) could be varied between $20^{\times}$ and $80^{\times}$ by changing the distance between the imaging lens and the digital camera. The magnification M was measured with a standard test pattern (with a line spacing of 10 μm) placed in place of the microplasma.

Figures 2a–2e show the interference patterns of the laser microplasma of the air recorded for different time delays of the probe pulse relative to the time of initial gas breakdown by exciting pulses with a peak ('in-vacuum') intensity $I \simeq (1 - 2) \times 10^{16}$ W cm^{-2}. Similarly to the case of plasma excitation by picosecond pulses [1, 2], the recorded interference patterns show the existence of three stages of formation and development of a femtosecond laser microplasma: the stage of primary gas ionisation (optical breakdown) and emergence of 'cold' plasma in the caustic of the focused beam (the so-called plasma filament, whose minimal transverse dimensions agree closely with the dimensions of the beam waist of exciting beam); the stage of efficient interaction between the resultant plasma and the exciting radiation, which lasts till the instant of laser pulse

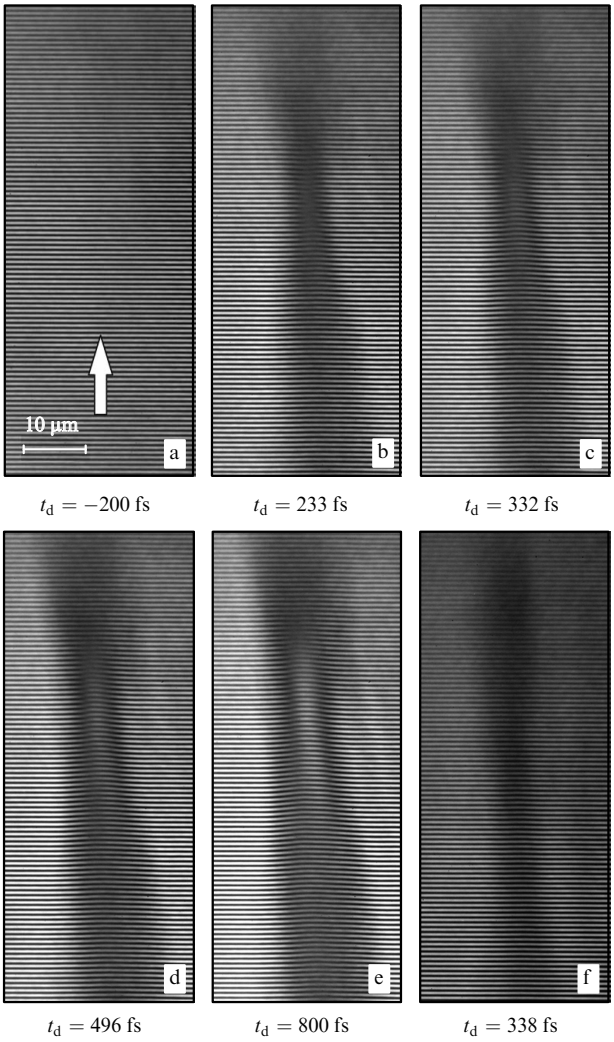

Figure 2. Interference patterns of a femtosecond laser plasma for different time delays t_d of the probe pulse relative to the instant of initial gas breakdown recorded in the air for an exciting pulse intensity $I \simeq (1-2) \times 10^{16}$ W cm^{-2} (a–e) and in helium for $I \simeq 8 \times 10^{16}$ W cm^{-2} (f). The arrow indicates the direction of exciting pulse propagation.

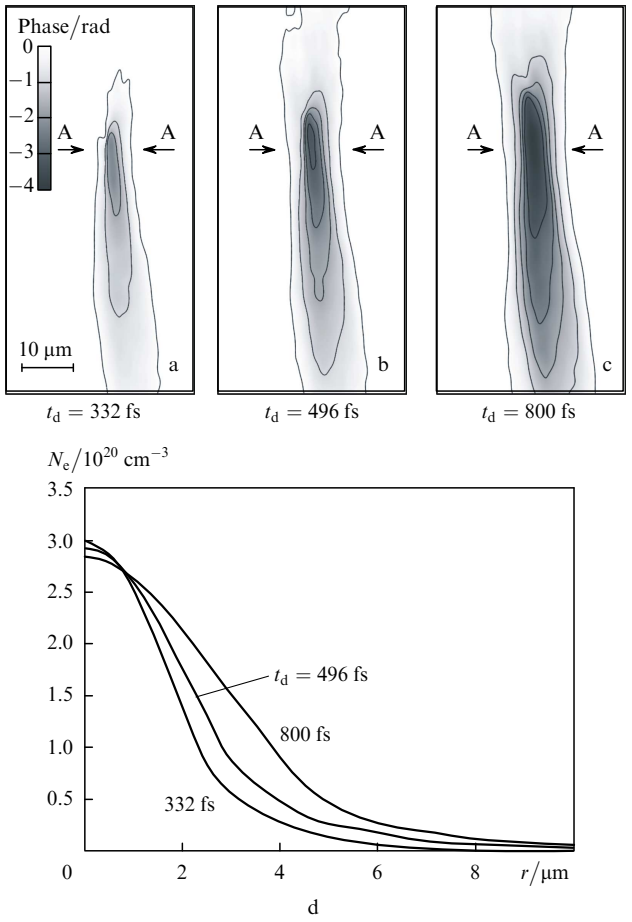

Figure 3. Phase distributions of the probe pulse for different time delays (a–c) reconstructed from the interference patterns of Figs 2c–2d and microplasma electron density distributions at radial sections AA (d).

cessation and is accompanied with laser radiation absorption, intense heating, and a fast expansion of the plasma filament; and the stage of free plasma expansion with a substantially lower (by an order of magnitude) expansion velocity. In this case, the main distinction of the spatial femtosecond microplasma structure from the picosecond one is its axial symmetry and the absence of expanding plasma object in the form of a 'bubble', which emerges at the picosecond plasma centre and propagates upstream of the laser radiation [1, 2].

Figure 2f shows the interference pattern of helium laser microplasma, which exhibits a substantially smaller distortion (bend) of interference fringes, which is due to a significantly lower electron density of the helium plasma in comparison with the air plasma and, as a consequence, a lower induced refractive index and a weak phase perturbation of the probe pulse.

Figures 3a–3c show the spatial phase distributions of the pro-be pulse upon its passage through the microplasma, which were derived from the above interference patterns. The pha-se reconstruction was performed using a conventional Fourier algorithm [29, 30] and the freely distributed IDEA (Interferometric Data Evaluation Algorithms, http://optics.tu-graz.ac.at/idea/idea.html) software.

The spatial phase distributions recorded permit reconstructing the spatial distribution of the refractive index in the laser microplasma with the use of a standard procedure involving the inverse Abelian transformation with the additional assumption of axial plasma symmetry, which is commonly made in these cases.

As is well known, the main cause of the change of the refractive index in laser-produced plasma is the 'negative' contribution of free electrons, which is responsible for the lowering of its refractive index to values below unity. Within the framework of the Drude model, the relationship between the variable electron plasma density $N_e(t)$ and the refractive index $n(t)$ is described by the well-known expressions:

$$n(t) = \left\{ n_0^2 - \left[\frac{\omega_p(t)}{\omega} \right]^2 \right\}^{1/2}, \quad \omega_p^2(t) = \frac{N_e(t) e^2}{\varepsilon_0 m_e}, \qquad (1)$$

where $\omega = 2.35 \times 10^{15}$ rad s^{-1} is the angular frequency of the probe radiation ($\lambda = 800$ nm); t is the time; $\omega_p(t)$ is the plasma frequency; e and m_e are the electron charge and mass; ε_0 is the permittivity of free space; and n_0 is the refractive index of the unperturbed gas.

The radial electron density distributions of the femtosecond air microplasma (at the section corresponding to the highest plasma density) at different stages of its development are plotted in Fig. 3d. The obtained data testify to an

extremely high degree of microplasma ionisation even at the stage of its interaction with the exciting pulse. The plasma density at the focus immediately after the passage of the high-intensity laser pulse amounts to $\sim 3 \times 10^{20}$ cm^{-3}, which is quite close to the highest possible (at atmospheric pressure) electron plasma density N_e^{max} of the fully ionised (up to the nuclei) air, which is equal to $\sim 3.6 \times 10^{20}$ cm^{-3}. So high an electron density emerges in the femtosecond air plasma when the exciting pulse intensity exceeds $\sim 10^{16}$ W cm^{-2}. In the case of excitation of helium, an almost complete ionisation of the gas was recorded for an intensity $I \simeq 4 \times 10^{16}$ W cm^{-2}. (The highest possible electron density in the case of helium was $N_e^{max} \simeq 5\times\ 10^{19}$ cm^{-3}.)

A lowering of the refractive index in laser plasma relative to the refractive index of the unexcited gas it typical for experiments of this kind. At the same time, in some region of the laser-produced air microplasma (Fig. 4) we recorded a significant increase of the refractive index up to values exceeding unity. This effect was observed in a rather narrow interval of time delays of the probe pulse ($t_d \simeq 20 - 100$ fs) relative to the onset of breakdown, i.e. only in the presence of the plasma-producing high-intensity laser radiation. The addition Δn to the refractive index was as high as ~ 0.04, and the total refractive index was equal to ~ 1.04, which substantially exceeded its value for the ambient air ($n_0 \simeq 1.000278$).

One possible cause of the emergence of a positive addition to the plasma refractive index is the abnormally high optical Kerr nonlinearity induced by the strong laser field, which has not been observed in a laser plasma. In the numerous papers dedicated to the study of the optical Kerr nonlinearity of a laser plasma (see, for instance, Refs [31, 32] and references therein), the highest measured values of the nonlinear refractive index n_2 were equal to $\sim 5\times 10^{-19}$ cm^2 W^{-1} [32]. Our estimates suggest that n_2 in our experiments may be several times higher than the above value.

In conclusion we note that the increase of the refractive index in the femtosecond ablation plasma of an aluminium target, which was first observed in Ref. [27], could not be related to the optical Kerr nonlinearity, because it manifested itself hundreds of picoseconds after the cessation of the laser pulse.

It is not improbable, however, that the increase of the refractive index detected may be due to the spatio-temporal limitations of the setup employed in experiments for recording the interference images.

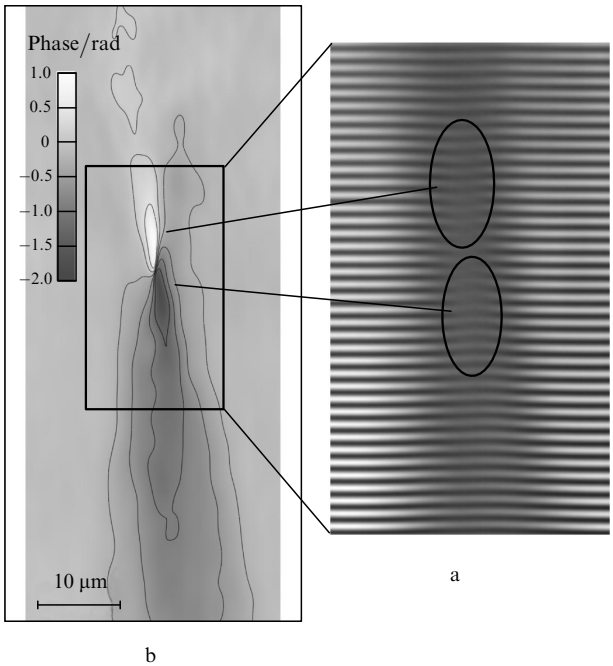

Figure 4. Interference pattern of a femtosecond air microplasma recorded during a high-intensity ($I \simeq 2 \times 10^{16}$ W cm^{-2}) exciting laser pulse (a) and reconstructed phase of the probe radiation (b). The positive change of phase may be indication that there exist plasma regions with a refractive index exceeding unity.

3. Ultrafast spectral-temporal diagnostics of femtosecond laser microplasma

Along with the study of the spatio-temporal structure as well as the measurements of the profiles of the refractive index and the electron density of the femtosecond laser microplasma, we investigated the spectral-temporal dynamics of microplasma radiation in the UV and visible spectral ranges at the initial stage of its formation and development – from the instant of laser spark initiation (the emission of continuum) to the emergence and development of individual spectral lines. Since the plasma emission in the form of spectral continuum sets in even in the presence of the exciting laser pulse (femtosecond in our case) and the physical processes that determine the development and transformation of the continuum are characterised, generally speaking, by ultrashort (pico- and subnanosecond) times, the top priority experimental task was to develop a method for ultrafast spectral-temporal diagnostics complying with the requirements of temporal resolution and spectral responsivity. For this purpose we adopted a method for the investigation of fast processes and the recording of weak light signals which involves the use of fast streak cameras (SCs) [33, 34].

Figure 5 shows the scheme of the proposed and experimentally realised method of ultrafast spectral-temporal diagnostics of the femtosecond laser microplasma. Single

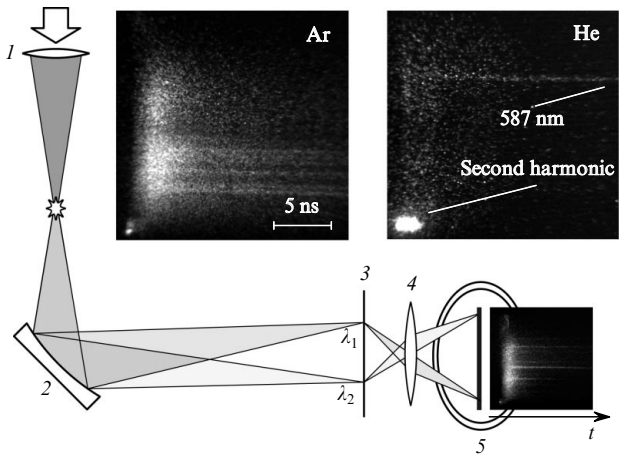

Figure 5. Scheme of the experiment on studying the ultrafast spectral-temporal dynamics of the femtosecond laser plasma by using a streak-camera: (*1*) focusing objective lens ($F = 8$ mm, NA = 0.5); (*2*) concave diffraction grating; (*3*) image plane of the diffraction grating ($\lambda_1 < \lambda_2$); (*4*) imaging lens; (*5*) SC. The insets show the dynamic spectra of Ar and He plasmas.

pulses of the previously described Ti : sapphire laser were focused with an aspherical microlens ($F = 8$ mm, NA = 0.5) to an intensity $I \simeq (0.9 - 2.5) \times 10^{17}$ W cm^{-2} and produced plasmas in the gases under investigation (the air, nitrogen, argon, helium) at atmospheric pressure. An axially arranged concave diffraction grating formed spatially separated spectral microplasma images, which were imaged with the requisite magnification onto the SC photocathode and swept in time. The mutually perpendicular arrangement of the spectrometer dispersion plane and the SC sweep direction afforded the observation of two-dimensional spectral-temporal pictures of the plasma emission.

In our experiments, use was made of a SC developed at the A.M. Prokhorov General Physics Institute, Russian Academy of Sciences [6, 33, 34]. This SC possessed a high spectral responsivity (2.1 mA W^{-1} at $\lambda = 800$ nm, an S1 photocathode) and a sufficiently broad dynamic range (no less than 10), which allowed us to reliably record and study the spectral-temporal dynamics of the femtosecond plasma emission in a broad wavelength range ($\lambda \simeq 300 - 1100$ nm) with a temporal resolution of $\sim$2.4 ps for a sweep speed up to $\sim 5 \times 10^9$ cm s^{-1}.

Figure 6a shows the time-swept emission spectra of the femtosecond laser plasma emerging in the optical breakdown of nitrogen and its tabulated ('statistical') line emission spectra (NIST Atomic Spectra Database, http://physics.nist.gov.PhysRefData/ASD/). One can see from these data that the plasma emission during the initial stage of its development, which is generally rather lengthy and may last hundreds and thousands of picoseconds after the onset of plasma formation, is a spectral continuum. Individual spectral lines (at least in the visible range under investigation, $\lambda \simeq 380 - 660$ nm) begin to show up only several nanoseconds later, as the plasma cools down. As is emerging from the continuum, the initially broad lines narrow rapidly and change in intensity. As this takes place, some lines that are relatively intense in 'statistical' spectra are relatively weak in the dynamic plasma spectra presented. By contrast, some 'dynamically' rather bright lines hardly show in the time-integrated spectra. This is evidently related to the existence of fast and slow radiative recombination processes in nonequilibrium plasmas.

The dynamic picture of plasma spectra formation presented in Figs 5 and 6 (the dynamic emission spectra of the laser-produced argon and helium plasmas are shown in the insets in Fig. 5) is not only quite illustrative, but is also rather informative to serve as a substantial basis both for a qualitative and quantitative theoretical analysis of the processes occurring in the extremely nonequilibrium laser plasma. In particular, from the variation of spectral line widths one can endeavour to estimate the plasma temperature and its cooling rate, while from line intensity ratios and line decay to estimate the rates of the corresponding recombination processes.

Figures 6c and 6d show examples of the temporal intensity variation of a nitrogen spectral line array (near

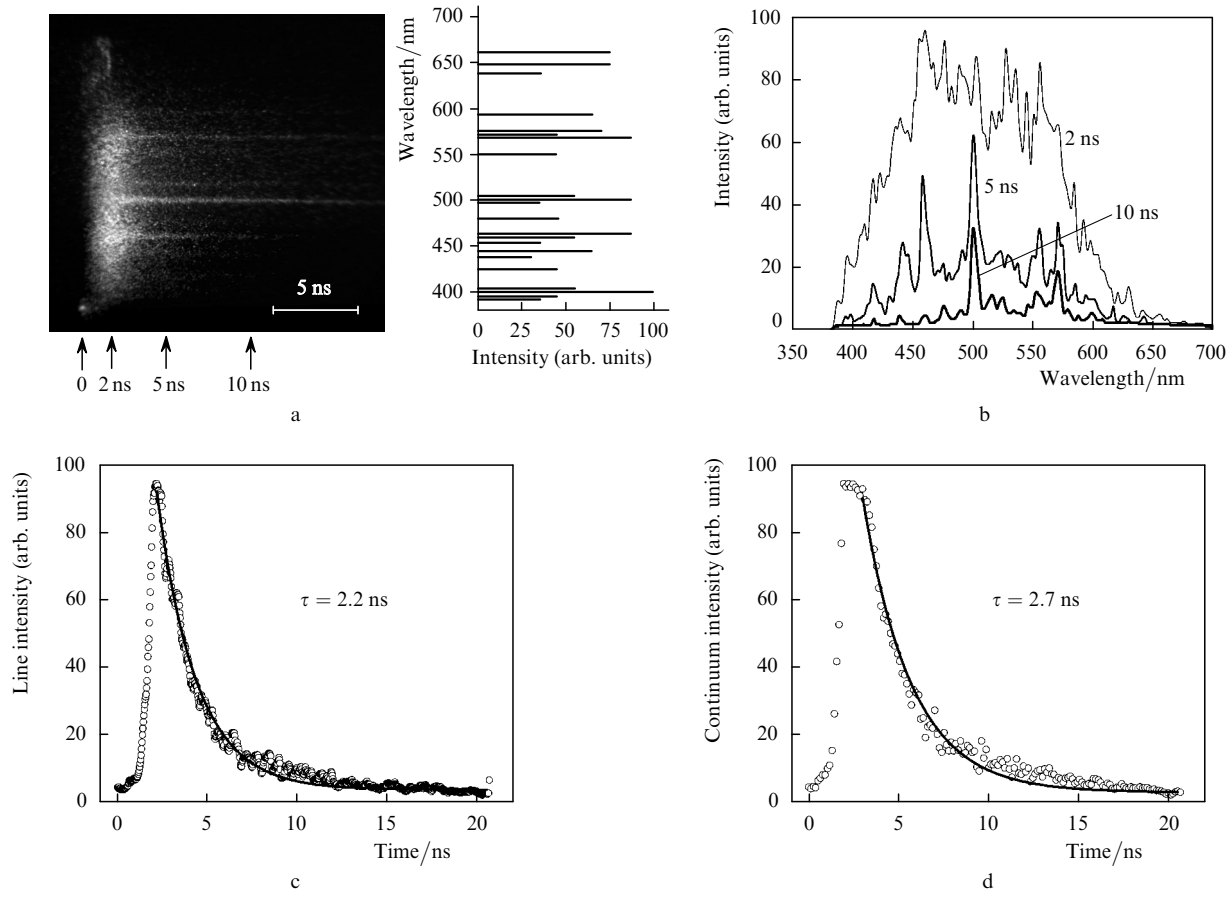

Figure 6. Spectral-temporal dynamics of femtosecond laser nitrogen plasma (at atmospheric pressure): time sweep of the spectra of the femtosecond plasma and 'static' nitrogen spectra in the $\lambda \simeq 380 - 660$ nm range (a), plasma emission spectra at different instants of time (b), temporal intensity dependences of the spectral lines and spectral continuum near $\lambda = 500$ nm (τ is the characteristic intensity decay time) (c, d).

$\lambda \simeq 500$ nm) and the variation of continuum intensity (in the region between the neighbouring lines), which decay with characteristic times τ of the order of several nanoseconds. Figure 6b shows the spectral profiles of nitrogen plasma emission recorded during the 0–10 ns time interval. It is evident that the absolute line intensities as well as the intensity ratios between different spectral components vary in the course of plasma development.

Because a comprehensive analysis of the resultant data does not come within the province of the present paper, we only note that until the present time the pursuance of an adequate analysis of the spectra of extremely nonequilibrium (in particular, femtosecond) laser plasmas and the ultrafast processes occurring therein has been largely limited by the lack of necessary experimental data similar to those obtained in the present work. In the preceding papers concerned with the investigation of the dynamics of the spectral composition of laser plasma emission in the visible range, the temporal resolution ranged mainly into the nano- and microseconds (see, for instance, Refs [35, 36]). This did not permit studying in detail the most interesting and least studied initial stage of plasma formation and development.

Another significant experimental result obtained in the present work is the observation of second (even) harmonic generation of femtosecond laser pulses in the optical gas breakdown plasma. The second (plasma) harmonic was recorded in all four media investigated – the air, nitrogen, argon, and helium. The electron-optical (streak) images of the optical spectra shown in Figs 5 and 6, the second harmonic has the appearance of a glowing point-like region whose location on the spectral scale corresponds to half the wavelength of exciting laser radiation ($\lambda/2 = 800$ nm$/2 =$ 400 nm) and on the temporal scale coincides with the plasma-generating femtosecond laser pulse. Despite the fact that the limited temporal resolution of the streak camera does not permit measuring the duration of the second harmonic and studying the dynamics of its formation (the durations of harmonic and femtosecond laser pulses recorded by the streak camera are essentially its $\sim$2.4-ps wide instrumental functions) and the spectral resolution limited by the diffraction grating does not permit to investigate in detail the spectral structure of the second harmonic, the very fact of its detection is beyond question. As far as we know, the observation of the second harmonic of femtosecond laser pulses in subcritical-density plasmas emerging in the optical gas breakdown had not been reported in the literature prior to our experiments. This circumstance appears to be surprising and even paradoxical considering the truly huge number of experimental and theoretical papers dedicated to the investigation of the processes and mechanisms involved in the generation of laser harmonics of higher (up to several hundred) odd orders by precisely the femtosecond pulses in the plasma of gases. Furthermore, earlier the second laser harmonic was comprehensively studied and experimentally observed in the gas plasma produced by picosecond pulses [37–40]. This circumstance is supposedly attributable to a significant difference (by orders of magnitude) in the efficiency of radiation conversion to odd and even harmonics (we are reminded that even harmonic generation is forbidden within the framework of the dipole approximation in a spatially uniform nonmagnetic plasma) and, as a consequence, to the necessity of employing in experiments substantially more sensitive methods of recording weak optical signals, to which the above electron-optical recording method belongs.

Within the framework of the present paper, a detailed study was made of the time-integrated spatial intensity distributions of the second harmonic. To this end, we used a Hamamatsu C4880 CCD camera. An axially arranged projection lens ($F = 8$ mm, NA $= 0.5$) imaged onto its sensitive matrix the region near the focal plane of the focusing objective lens (the plasma formation region), which corresponded to the smallest transverse size of the second harmonic beam. Our experiments revealed that this region corresponded to the position of the waist of the plasma-generating laser beam.

Figure 7 shows the spatial intensity profiles of the second harmonic radiation and the initial laser beam at its waist. Because of the initial ellipticity of the Gaussian spatial profile of the output Ti : sapphire laser radiation, the

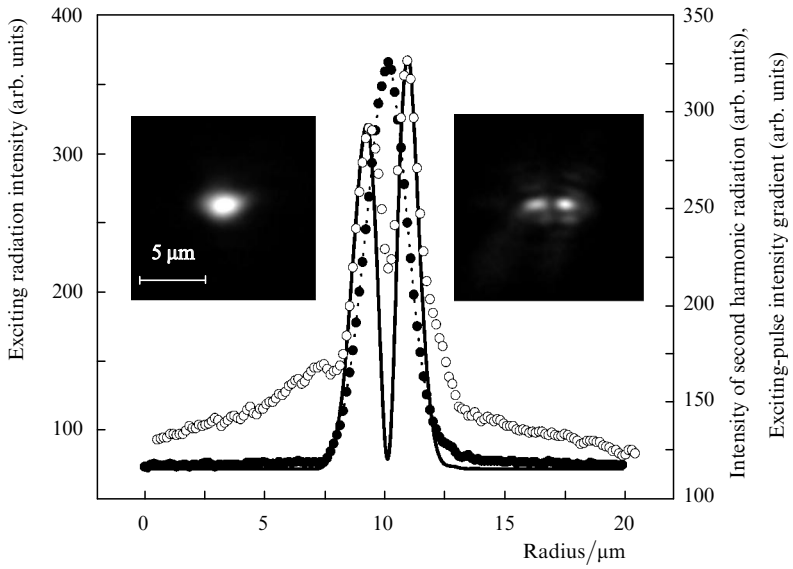

Figure 7. Images (in the insets) and spatial intensity distributions of the focused laser pulse (●) and the second harmonic radiation (○) generated in the air microplasma. The solid curve represents the intensity gradient for the exciting pulse.

measured profile of the focused beam at the waist also exhibited a characteristic ellipticity and measured $\sim 2.5 \times 3.5$ μm (at the $1/e^2$ level). The plane of incident radiation polarisation coincided with the major axis of the ellipse. The images of the initial radiation and second harmonic beams depicted in Fig. 7 as well as their intensity distributions at the section along the major axis of the ellipse show the characteristic spatial structure of the second harmonic with two intensity peaks aligned with the direction of the plane of exciting beam polarisation. In this case, the intensity profile of second harmonic radiation at its intensity maxima agrees nicely with the profile of the intensity gradient of the exciting radiation in the plane of polarisation.

The above facts are indicative of the realisation of one of the possible mechanisms of second harmonic generation in a laser plasma with a spatially nonuniform density distribution, which was proposed in Ref. [37] and subsequently elaborated in Refs [38–40]. In Refs [37, 38] it was theoretically shown that the prohibition of second harmonic generation in subcritical-density plasmas is removed in the presence of a gradient of the refractive index and that such a plasma may be a source of radiation at the double frequency owing to the presence of a nonvanishing term with the second-order nonlinear susceptibility in the induced nonlinear polarisation. In Ref. [38], a simple expression was derived for the vector of plasma polarisation at the double frequency in a laser field with a Gaussian spatial radiation distribution:

$$\boldsymbol{P}(2\omega) = \left[2s\chi_{\mathrm{fe}}^{(2)}(2\omega)/w_0^2\right]\left[E^2\boldsymbol{r} - 4\boldsymbol{E}(\boldsymbol{E}\boldsymbol{r})/\varepsilon_{\mathrm{p}}\right], \qquad (2)$$

where $\boldsymbol{E}$ is the electric field intensity; $\chi_{\mathrm{fe}}^{(2)}(2\omega)$ is the nonlinear susceptibility of the second order; s is a numerical coefficient characterising the mechanism of primary gas ionisation; ε_{p} is the plasma permittivity; w_0 and $\boldsymbol{r}$ are the waist radius and the radial coordinate of the Gaussian beam. Relationship (2) perfectly describes all the features of second harmonic generation observed in our experiments: the existence of two spatial intensity peaks and their orientation along the plane of polarisation of the initial laser field, the correspondence of the spatial harmonic-radiation intensity profile to the gradient of the exciting-beam intensity profile (and therefore the correspondence to the plasma density gradient, as noted in Section 2), the complex polarisation structure of the second harmonic, which is a superposition of a mostly linearly polarised (in the same plane as the initial beam) component and a small fraction of radially polarised radiation [38].

Therefore, the mechanism of second harmonic generation in subcritical-density plasma, which was proposed long before the emergence of the first femtosecond lasers and which implies only the presence of an appreciable density gradient of the plasma refractive index, has supposedly been borne out in our experimental investigations.

4. Conclusions

We have developed a method for the ultrafast precision interferometric diagnostics of the spatio-temporal dynamics of a micrometre-sized laser plasma emerging in the optical breakdown induced by high-intensity ($I = 10^{14}$–10^{17} W cm^{-2}) tightly focused femtosecond pulses of a Ti : sapphire laser ($\lambda = 800$ nm, $\tau_{\mathrm{p}} \simeq 130$ fs). Measurements were first made of the instantaneous distributions of the refractive index and the electron density in a subcritical-density femtosecond laser microplasma in the air and helium with a micrometer spatial resolution during the exciting laser pulse.

We have proposed and experimentally realised a new electron-optical (streak) technique for the ultrafast spectral-temporal recording of plasma radiation and nonlinear-optical laser radiation conversion. This technique enabled us for the first time to investigate with a picosecond temporal resolution the dynamics of the formation and development of the spectral continuum and spectral lines in a femtosecond laser plasma in gases (the air, nitrogen, argon, helium) and to record for the first time the generation of the second (even) harmonic of femtosecond laser pulses in a subcritical density plasma.

Acknowledgements. This work was done under the auspices of the 'Femtosecond Optics and New Optical Materials' Program of the Presidium of the Russian Academy of Sciences, the 'Optical Spectroscopy and Frequency Standards' Program of the Physical Sciences Division of the Russian Academy of Sciences, and the Russian Foundation for Basic Research (Grant No. 06-02-17014).

References

1. Garnov S.V., Konov V.I., Malyutin A.A., Tsarkova O.G., Yatskovskii I.C., Dausinger F. *Kvantovaya Elektron.*, **33** (9), 758 (2003) [*Quantum Electron.*, **33** (9), 758 (2003)].
2. Garnov S.V., Konov V.I., Malyutin A.A., Tsarkova O.G., Yatskovsky I.S., Dausinger F. *Laser Phys.*, **13** (3), 386 (2003).
3. Garnov S.V., Bukin V.V., Vorobiev N.S., Malyutin A.A., Konov V.I., Schelev M.Ya. *Techn. Dig. of Int. Conf. on Coherent and Nonlinear Optics (ICONO/LAT'2005)* (St. Peterburg, 2005) IWJ2.
4. Garnov S.V., Bukin V.V., Malyutin A.A., Konov V.I., Vorobiev N.S., Schelev M.Ya. *Proc. Int. Symp. on Topical Problems of Nonlinear Wave Physics (NWP-2005)* (St. Peterburg, N. Novgorod, 2005) p. 45.
5. Garnov S.V., Konov V.I., Lozovoi V.I., Malyutin A.A., Schelev M.Ya., Vorobiev N.S. *Conf. Programm of Int. Symp. on Modern Problems of Laser Physics (MPLP'04)* (Novosibirsk, 2004).
6. Garnov S.V., Konov V.I., Lozovoi V.I., Malyutin A.A., Schelev M.Ya., Vorobiev N.S. *Proc. SPIE Int. Soc. Opt. Eng.*, **5580**, 811 (2005).
7. Belland P., De Michelis C., Mattioli M. *Opt. Commun.*, **3**, 7 (1971).
8. Attwood D.T., Coleman L.W. *Appl. Phys. Lett.*, **24**, 408 (1974).
9. Azechi H., Oda S., Tanaka K., Norimatsu T., Sasaki T., Yamanaka T., Yamanaka C. *Phys. Rev. Lett.*, **39**, 1144 (1977).
10. Attwood D.T., Sweeney D.W., Auerbach J.M., Lee P.H.Y. *Phys. Rev. Lett.*, **40**, 184 (1978).
11. Attwood D.T. *IEEE J. Quantum Electron.*, **14** (12), 909 (1978).
12. Raven A., Willi O. *Phys. Rev. Lett.*, **43**, 278 (1979).
13. Vlasov N.G., Korchazhkin S.V., Matsonashvili R.B., Petryakov V.M., Sobolev S.S., Chalkin S.F. *Opt. Spektrosk.*, **59** (4), 934 (1985).
14. Da Silva L.B., Barbee T.W., Cauble R. Jr., Celliers P., Ciarlo D., Libby S., London R.A., Matthews D., Mrowka S., Moreno J.C., Ress D., Trebes J.E., Wan A.S., Weber F. *Phys. Rev. Lett.*, **74**, 3991 (1995).
15. Shao Y.L., Ditmire T., Tisch J.W.G., Springate E., Marangos J.P., Hutchinson M.H.R. *Phys. Rev. Lett.*, **77**, 3343 (1996).
16. Sarkisov G.S., Bychenkov V.Yu., Novikov V.N., Tikhonchuk V.T., Maksimchuk A., Chen S.-Y., Wagner R., Mourou G., Umstadter D. *Pis'ma Zh. Eksp. Teor. Fiz.*, **66** (12), 787 (1997).

17. Ditmire T., Gumbrell E.T., Smith R.A., Djaoui A., Hutchinson M.H.R. *Phys. Rev. Lett.*, **80** (4), 720 (1998).
18. Breitling D., Schittenhelm H., Berger P., Dausinger F., Hugel H. *Appl. Phys. A*, **69**, S505 (1999).
19. Sarkisov G.S., Bychenkov V.Yu., Novikov V.N., Tikhonchuk V.T., Maksimchuk A., Chen S.-Y., Wagner R., Mourou G., Umstadter D. *Phys. Rev. E*, **59**, 7042 (1999).
20. Edwards M.J., MacKinnon A.J., Zweiback J., Shigemori K., Ryutov D., Rubenchik A.M., Keilty K.A., Liang E., Remington B.A., Ditmire T. *Phys. Rev. Lett.*, **87**, 085004 (2001).
21. Couairon A., Berge L. *Phys. Rev. Lett.*, **88**, 135003-1 (2002).
22. Smith R.F., Dunn J., Nilsen J., Shlyaptsev V.N., Moon S., Filevich J., Rocca J.J., Marconi M.C., Hunter J.R., Barbee T.W. *Phys. Rev. Lett.*, **89**, 065004-1 (2002).
23. Garnov S.V., Malyutin A.A., Tsarkova O.G., Konov V.I., Dausinger F. *Proc. SPIE Int. Soc. Opt. Eng.*, **4637**, 31 (2002).
24. Kim K.Y., Alexeev I., Milchberg H.M. *Opt. Express*, **10** (26), 1563 (2002).
25. Tang H., Guilbaud O., Jamelot G., Ros D., Klisnick A., Joyeux D., Phalippou D., Kado M., Nishikino M., Kishimoto M., Sukegawa K., Ishino M., Nagashima K., Daido H. *Appl. Phys. B*, **78**, 975 (2004).
26. Richardson M., Koay C.-S., Takenoshita K., Keyser C., Bernath R., George S., Teerawattansook S. *Proc. SPIE Int. Soc. Opt. Eng.*, **5580**, 434 (2005).
27. Filevich J., Rocca J.J., Marconi M.C., Moon S.J., Nilsen J., Scofield J.H., Dunn J., Smith R.F., Keenan R., Hunter J.R., Shlyaptsev V.N. *Phys. Rev. Lett.*, **94** (3), 035005 (2005).
28. Giulietti A., Galimberti M., Gamucci A., Giulietti D., Gizzi L., Koester P., Laate L., Tomassini P., Vaselli M. *Techn. Dig. of Int. Conf. on Coherent and Nonlinear Optics (ICONO/LAT'2005)* (St. Peterburg, 2005) IWJ3.
29. Takeda M., Ina H., Kobayashi S. *J. Opt. Soc. Am.*, **72**, 156 (1982).
30. Nugent K. *Appl. Opt.*, **24**, 3101 (1985).
31. Vlasov D.V., Garaev R.A., Korobkin V.V., Serov R.V. *Zh. Eksp. Teor. Fiz.*, **49**, 1033 (1979).
32. Pennington D.M., Henesian M.A., Hellwarth R.W. *Phys. Rev. A*, **39**, 3003 (1989).
33. Shchelev M.Ya. *Trudy Fiz. Inst. Akad. Nauk SSSR*, **155**, 3 (1985).
34. Andreev A.N., Dubovik A.S., Degtyareva V.P., Monastyrskii M.A., Shchelev M.Ya. *Vysokoskorostnaya fotografiya i fotonika v issledovanii Bystroprotekayushchikh protsessov* (High-Speed Photography and Photonics in Investigations of Ultrafast Processes) Ed. by A.M. Prokhorov (Moscow: Logos, 2002) p. 464.
35. Yalcin S., Crosley D.R., Smith G.P., Faris G.W. *Appl. Phys. B*, **68**, 121 (1999).
36. Zeng X., Mao X., Mao S.S., Yoo J.H., Greif R., Russoa R.E. *J. Appl. Phys.*, **95** (3), 816 (2004).
37. Jha S.S. *Phys. Rev. Lett.*, **15**, 412 (1965).
38. Bethune D.S. *Phys. Rev. A*, **23**, 3139 (1981).
39. Malcuit M.S., Boyd R.W., Davis W.V., Rzaewski K. *Phys. Rev. A*, **41**, 3822 (1990).
40. Mullin C.S., Kim D., Feller M.B., Shen Y.R. *Phys. Rev. Lett.*, **74**, 2678 (1995).